PROCEEDINGS OF SCIENCE

Angular Resolution for the Radio Neutrino Observatory Greenland (RNO-G)

Ilse Plaisier[a,*] **for the RNO-G Collaboration**
(a complete list of authors can be found at the end of the proceedings)
[a] *DESY, Platanenallee 6, 15738 Zeuthen, Germany*
E-mail: ilse.plaisier@desy.de

In the ultra-high energy regime, the low predicted neutrino fluxes are out of reach for currently running neutrino detectors. Larger instrumented volumes are needed to probe these low fluxes. The Radio Neutrino Observatory Greenland (RNO-G) detects in-ice radio waves emitted by neutrino induced particle showers in the Greenlandic ice sheet. Radio waves have a large attenuation length in ice O(1 km) and therefore RNO-G implements a sparse instrumentation to cover an unprecedented volume. The first seven RNO-G stations have been deployed in the summer of 2021 and 2022 and deployment will be ongoing in the next years. This contribution discusses the angular resolution of RNO-G. We use a method that uses a parametrization for the emitted electric field which is forward folded through the detector and matched with the voltage traces as obtained in the antennas of an RNO-G station. We obtain a $\sigma_{68\%}$ angular resolution of 8° for an optimized event set (75%), and $\sigma_{68\%}$=3° for the subset of events which have significant signal strength in two antennas measuring perpendicular electric-field components, such that a good measurement of the polarization can be obtained.

9th International Workshop on Acoustic and Radio EeV Neutrino Detection Activities - ARENA2022
7-10 June 2022
Santiago de Compostela, Spain

*Speaker

PoS(ARENA2022)008

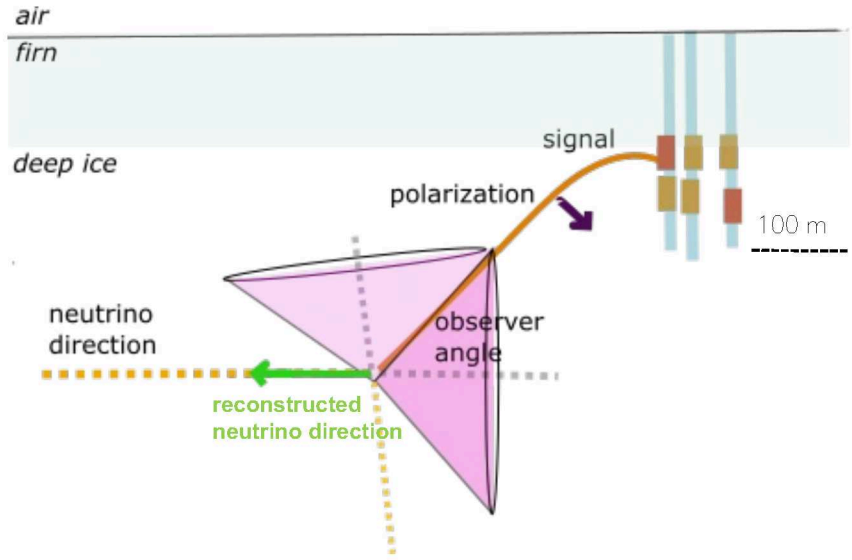

Figure 1: Sketch of the shower geometry for the radio emission of an in-ice neutrino interaction (not to scale). The radio emission is strongest on a wide cone (pink). The path of the radio emission detected at the station is drawn in orange. The polarization of the electric field is drawn with an arrow (purple). The observer angle, signal direction and polarization together enables pin-pointing of the neutrino direction.

1. Reconstructing the neutrino direction with RNO-G

The Radio Neutrino Observatory in Greenland (RNO-G) is a neutrino observatory, using the technique of detecting the radio emission generated by in-ice neutrino-induced particle showers with antennas. RNO-G aims for the detection of the first neutrino with an energy above 10 PeV, as its sensitivity ranges from 10 PeV to 10 EeV energies [1, Figure 24]. Antennas are located on 100 meter deep *strings*, clustered in 3 strings per *station* [1, Figure 7] and the stations located on a grid with a 1.25 km spacing [1, Figure 7]. Stations function and trigger autonomously, and are therefore located on a sparse grid to optimize the RNO-G effective volume. Hence, each station is designed to enable reconstruction of the neutrino properties, i.e. direction and energy.

The cosmic-ray flux is established up to 100 EeV, meaning that neutrinos with energies of EeV are expected as secondary particles due to the interaction of the cosmic rays with ambient matter in the sources of production and photon fields. Due to their chargeless nature, EeV neutrinos can be used to identify the sources of the highest energy cosmic rays, by reconstructing their direction. Furthermore, since no neutrino has been detected using the in-ice radio technique, reconstructing the direction is essential for the identification of the first *radio neutrino*.

The particle shower evolves a changing excess of negative charges during the development, which is the cause of the produced radio emission. The large density of the ice results in a slower speed of the radio emission than the particle shower. Hence, the radio signal is coherent on a broad cone, strongest on the Cherenkov angle ($\theta \approx 55.6°$). Radio emission observed at the detector, under the observer angle, can therefore originate from any location on this cone. A measure of the polarization of the electric field at the antenna is needed to pinpoint the neutrino direction, since the radio emission is known to be polarized in the direction of the shower axis. This is visualized in Figure 1. Therefore, the **signal direction**, **observer angle** and the **polarization angle** are needed to

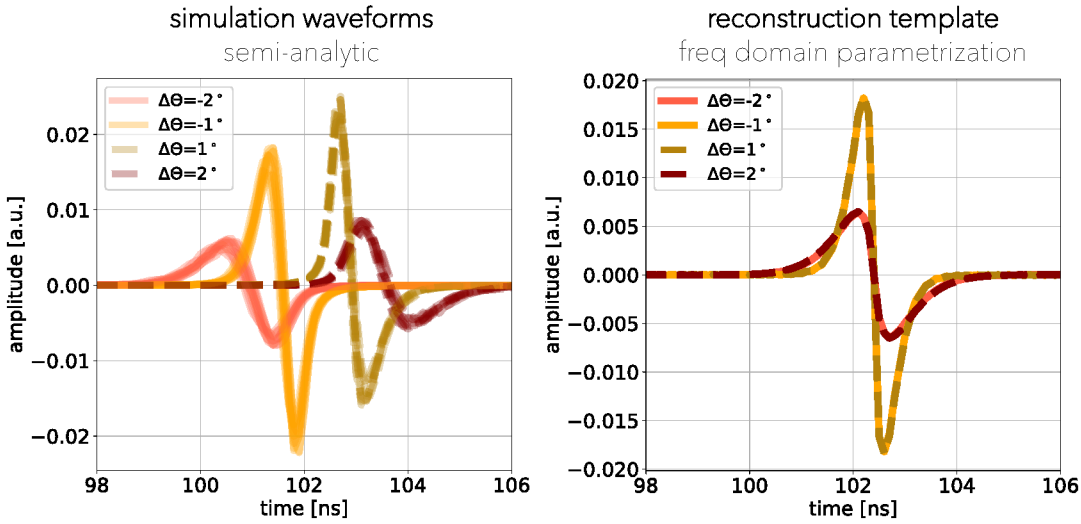

Figure 2: Electric-field pulses from neutrino induced in-ice particle showers. Shown are pulses 1° (yellow) and 2° (red) off on each side of the Cherenkov angle (≈55.6°). Left shows waveforms based on full particle shower simulations and right shows a frequency domain parametrization of the electric field as is used for the reconstruction.

reconstruct the neutrino direction. To measure the polarization the station is equipped with antennas measuring horizontal (Hpol) and vertically (Vpol) polarized electric-field components. The Hpol is much lower in gain than the Vpol due to the obligated vertical orientation of the antennas in the narrow (30 cm) boreholes.

2. Method to reconstruct the neutrino direction

For the reconstruction of the neutrino properties, an analytic description of the electric field is used which is forward folded through the propagation and system response to obtain voltage waveform templates. The templates are compared with the voltage data and a test statistic is minimized to obtain the neutrino direction corresponding to the best-fit template. This *forward folding* approach has shown to work better for reconstructing low signal amplitude radio pulses, than unfolding with the detector response [2]. Due to the contribution of thermal fluctuations in the voltage data, unfolding with the (noiseless) detector response overestimates the signal contribution when the detector response expects a low value, which is overcome by the comparison of the noiseless voltage templates obtained by the forward folding method. A similar forward folding method has been used for the ARIANNA near-surface station [3].
This model dependent approach requires a good electric-field model which can be directly related to the neutrino properties. Electric-field simulations are shown in Figure 2 left for observer angles 1° and 2° on each side of the Cherenkov angle. For the analytic model, the frequency domain parametrization from [4] is used which is shown in Figure 2 right and only depends on the **shower energy** and the **observer angle**. Due to lack of information of the individual shower profiles timing information is not available, i.e. assumed is that all frequency components arrive at the same time.

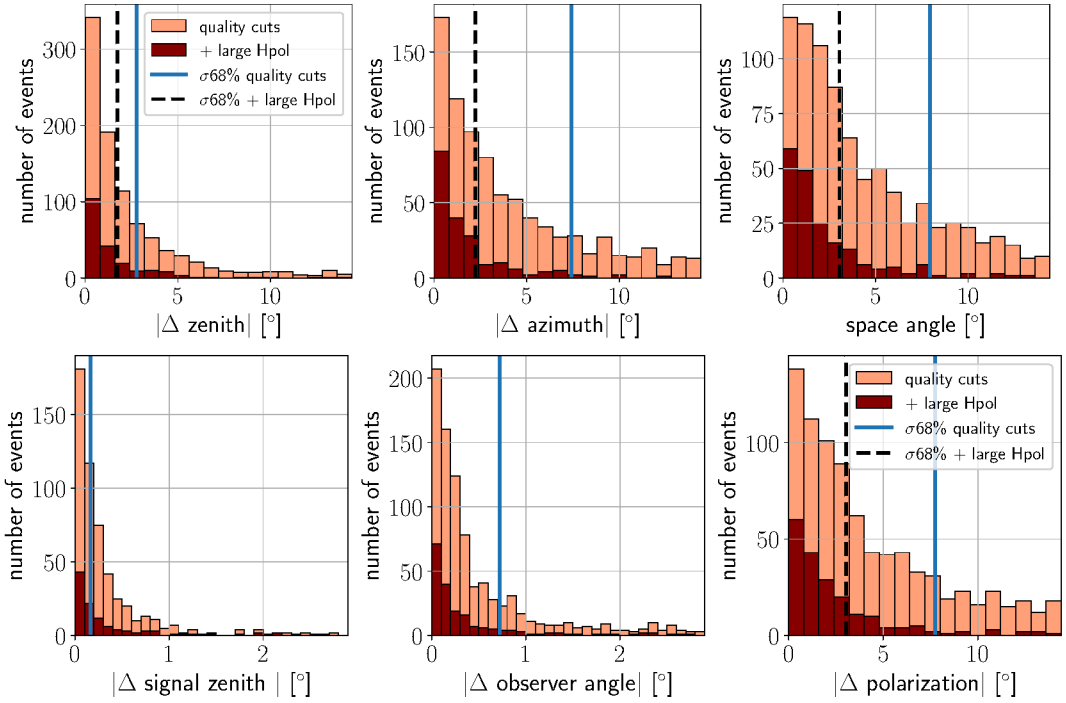

Figure 3: Resolutions of the parameters relevant for the neutrino direction for events passing the quality cuts (75%). Top: Distributions of the difference in true and best fit zenith position (left), azimuth position (middle) and direction (right). Bottom: Distributions of the difference in true and best fit signal direction (left), observer angle (middle) and polarization angle (right). Indicated in dark red are the events with a large contribution in the Hpol. The blue (black) line indicates the 68% containment (including Hpol cut).

Therefore, the model is symmetric around the Cherenkov angle as can be seen in the figure. Because off the Cherenkov angle the higher frequencies lose coherency, the shape of the pulse depends on the observer angle.

As a first step of the reconstruction procedure, the interaction point of the neutrino is reconstructed, which is needed to determine for a given neutrino direction the observer angle of the radio emission at the detector. The best fitted direction is then determined by a χ^2-minimization of the resulting templates for all pulses arriving in the antennas of a station.

Due to the loss of timing information in the template waveforms (pulses are delayed in time for $O(1\text{ ns})$ for $\Delta 1°$, see Figure 2) a correlation of the template with the data is performed to temporally match the template and data. Therefore, a selection criteria is used to cut out low amplitude pulses in order to avoid fitting the thermal noise, for which currently a simple amplitude threshold cut is used.

The station contains four 1 meter vertically separated Vpols, for which the waveforms are beamformed to function as a low threshold trigger. Beamforming of these waveforms is used in the reconstruction procedure to identify the pulse position in these antennas and the two Hpols directly above ([1, Figure 7]) and are therefore always included in the fit regardless of the amplitude cut.

The forward folding approach has the benefit that using more antennas in the same reconstruction effectively reduces the noise contribution and therefore improves the resolution. Furthermore, the

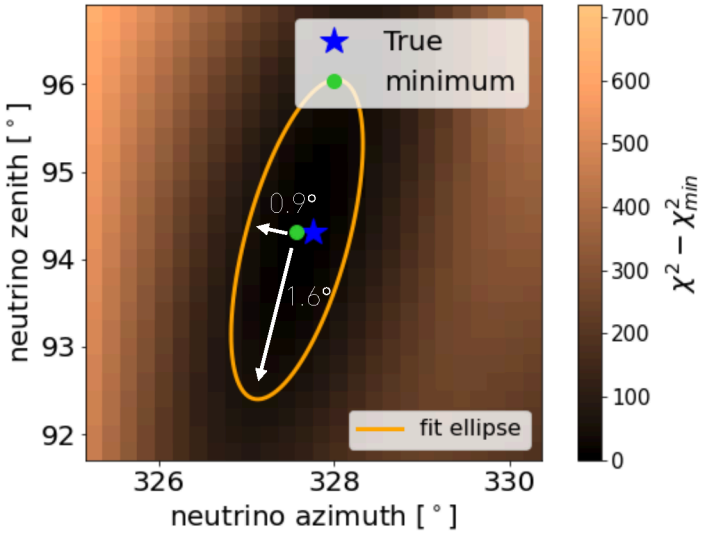

Figure 4: Minimization landscape around the best fit position for an example event with a large contribution in the Hpol. The true direction (blue star) and the best fit position (green dot) are indicated. The contour of $\chi^2_{\text{min}} + \chi^2_{68\%}$ is drawn such that it contains 68% or repeated experiments as obtained with simulations. The contour is fitted with an ellipse, for which the major and minor axis are given.

forward folding approach allows for the combination of antennas across the entire station, for which the vertical and horizontal spatial separation results in a more accurate measure of the polarization, besides a measured voltage in the Vpol and the Hpol.
A more detailed and technical explanation of the reconstruction procedure is described in [5] and [6].

3. Resulting angular resolution

The performance of the reconstruction method is evaluated with a simulation set obtained with NuRadioMC [7], representing an event-set triggering a single RNO-G station with a neutrino flux assumption of an extension of the IceCube flux [8] and the cosmogenic neutrino prediction from [9]. Quality cuts are applied to the event set that mainly filter out the low signal-to-noise ratio events, reducing the event set to 75%. Figure 3 top shows the angular difference of the true and reconstructed direction in zenith (left), azimuth (middle) and space angle (right). As seen, 68% of the events are reconstructed within 8° with a significant improvement for events with a large contribution in the Hpol since it results in a better polarization reconstruction, reducing to 3°. Furthermore, a better resolution in zenith than azimuth is obtained, which is due to the geometry of the in-ice radio cone that causes mainly the upper part of the Cherenkov cone to trigger an RNO-G station.
Shown in Figure 3 bottom are the resolutions for the signal direction, observer angle and polarization. Clearly seen is that the largest contribution to the space angle is the uncertainty in polarization.

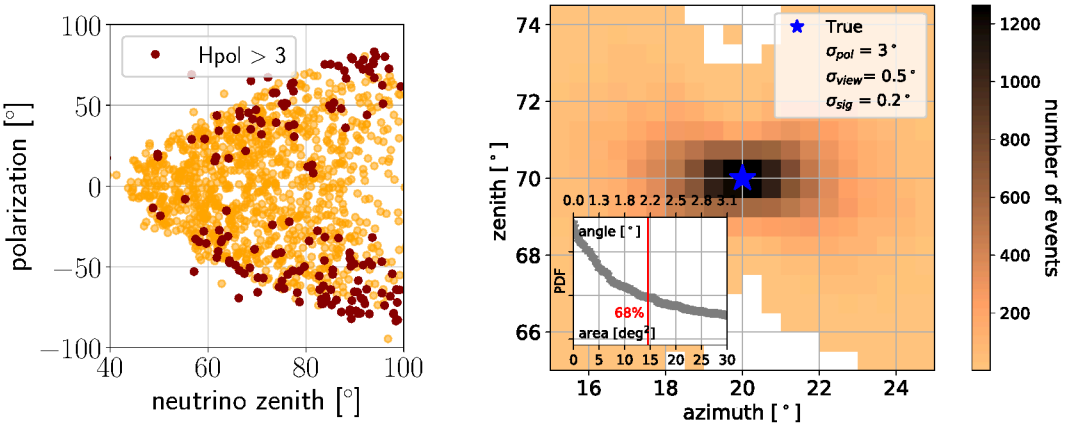

Figure 5: Left: Relation for the neutrino zenith direction and the polarization angle. A broader distribution of polarization angles is observed for inclined directions. Right: Distribution of best fit points (point spread function) for a source position of 70°. Assumed are Gaussian uncertainties on the observer angle, polarization and signal direction, as indicated in the figure. The inset figure shows the 1D distribution for equivalent area coverage.

4. Event contours and the point spread function

Since the largest contribution of the resolution comes from the polarization uncertainty, the **event contours** result in a long narrow region on a cone and therefore are very asymmetric. A 68% containment area of 9 deg^2 is obtained for a signal direction $\sigma_{68\%}$ = 0.2°, observer angle of $\sigma_{68\%}$ = 0.5° and polarization of $\sigma_{68\%}$ = 3° for Gaussian uncorrelated uncertainties. Figure 4 shows the results of the χ^2-calculation on a grid around the reconstructed direction with the 68% contour. This example shows an event with a large contribution in the Hpol, resulting in a good reconstruction of the polarization. As can be seen, the contour is ellipse-like. For uncorrelated resolutions in viewing and polarization, the major and minor axis of the ellipses can be approximated with these resolutions due to the small signal direction resolution. An improvement in observer angle resolution is obtained for larger amplitude Vpol, whereas the polarization mainly depends on the amplitude in the Hpol.

The geometry of the shower forbids vertically arriving neutrinos from triggering an RNO-G station. For an arrival direction of zenith ≈40° the top of the radio-cone can be observed, and a more broad range of the cone will be detectable for more inclined showers. This results in a polarization angle distribution as shown in Figure 5 left. In other words, more inclined showers result in a larger allowed parameter space of interaction points in the ice that result in triggering the RNO-G station and therefore a broader parameter space for polarization angles as observed at a detector. Hence, neutrinos as observed from a source at different inclinations, result in a broader source **point spread function** for more inclined showers. The point spread function for a source at zenith of 70° is shown in Figure 5 right, assuming Gaussian uncorrelated uncertainties on the polarization (σ=3°), observer angle (σ=0.5°) and signal direction (σ=0.2°).

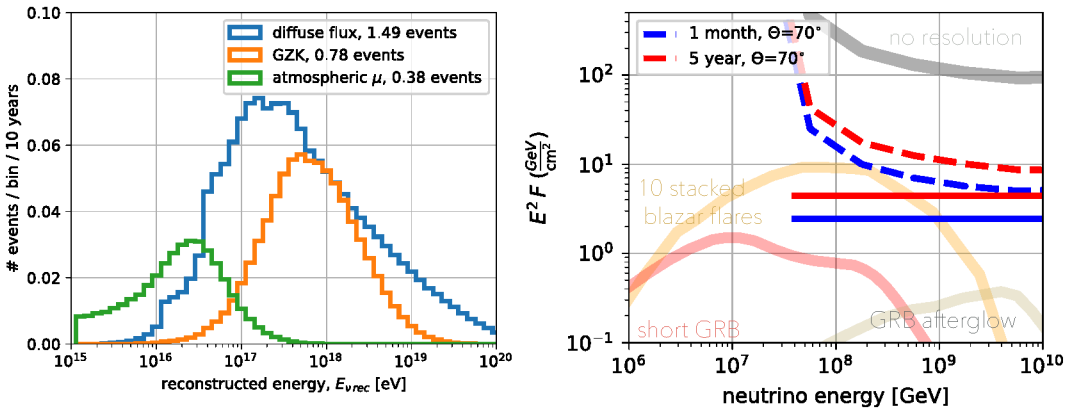

Figure 6: Left: Number of detected events for 10 years of 35 RNO-G stations for a diffuse neutrino flux model (an extension of the IceCube flux [8] and cosmogenic neutrinos [9]) and atmospheric muons [10]. Right: The fluences required for RNO-G for a 5-σ neutrino discovery of a point source (discovery potential) for a 5 year (steady source, red) and a 1 month (transient, blue) integration time, compared to fluences of models of blazars (6 month) [11] , a GRB (seconds) [12] and a GRB afterglow (35 days) [13] . The discovery potential is calculated using the background assumption from the left figure.

5. Resulting discovery potential

Pinpointing neutrinos detected with RNO-G to their direction of origin, allows for the identification of the sources producing the neutrinos. The obtained angular resolution is used to calculate the neutrino fluence required from a source such that RNO-G is capable of identifying the signal events above the background events. The mimicked analysis is searching the sky around a point source and identifying the number of neutrinos required to identify the source above the diffuse background (diffuse astrophysical [8], cosmogenic [9] and muons [10]). Assumed is here that muons will not be vetoed by detecting cosmic rays in the surface detector, and therefore the background assumption is overestimated [14]. Background numbers contain large systematic uncertainties since the muon background as well as the neutrino flux at these energies are unmeasured. Figure 6 left shows the expected number of events for RNO-G in 10 years of live time, which function as the background events for the point source analysis. Figure 6 right shows the 5-σ fluence required in 50% of the experiments to identify a source at an inclination of 70° assuming a source energy behavior of an E^{-2} spectrum, i.e. the 5-σ discovery potential, as calculated with [15]. Estimates are conservative, as a symmetric point spread function is assumed based an on the space angle distribution in Figure 3, which is overestimating the area (i.e. background number). Statistics from RNO-G will likely be too low to identify individual sources in the next few years, unless in multi-messenger context.

References

[1] RNO-G collaboration, *Design and Sensitivity of the Radio Neutrino Observatory in Greenland (RNO-G)*, *JINST* **16** (2021) P03025 [2010.12279].

[2] C. Glaser, A. Nelles, I. Plaisier, C. Welling, S. W. Barwick, D. Garcia-Fernández et al., *NuRadioReco: a reconstruction framework for radio neutrino detectors*, *The European Physical Journal C* **79** (2019) .

[3] G. G. Gaswint, *Quantifying the Neutrino Energy and Pointing Resolution of the ARIANNA Detector*, Ph.D. thesis, UC, Irvine, 2021.

[4] J. Alvarez-Muniz, A. Romero-Wolf and E. Zas, *Practical and accurate calculations of Askaryan radiation*, *Phys. Rev. D* **84** (2011) 103003 [1106.6283].

[5] I. Plaisier, S. Bouma and A. Nelles, *Reconstructing the arrival direction of neutrinos in deep in-ice radio detectors*, . **in preparation** .

[6] I. Plaisier, *Reconstructing the arrival direction of cosmic neutrinos with the Radio Neutrino Observatory Greenland (RNO-G)*, Ph.D. thesis, Friedrich-Alexander-Universität, Erlangen-Nürnberg, 2022.

[7] C. Glaser et al., *NuRadioMC: Simulating the radio emission of neutrinos from interaction to detector*, *Eur. Phys. J. C* **80** (2020) 77 [1906.01670].

[8] IceCube collaboration, *Improved Characterization of the Astrophysical Muon–neutrino Flux with 9.5 Years of IceCube Data*, *Astrophys. J.* **928** (2022) 50 [2111.10299].

[9] A. van Vliet, R. A. Batista and J. R. Hörandel, *Determining the fraction of cosmic-ray protons at ultrahigh energies with cosmogenic neutrinos*, *Physical Review D* **100** (2019) .

[10] D. Garcia-Fernández, A. Nelles and C. Glaser, *Signatures of secondary leptons in radio-neutrino detectors in ice*, *Physical Review D* **102** (2020) .

[11] K. Murase, Y. Inoue and C. D. Dermer, *Diffuse neutrino intensity from the inner jets of active galactic nuclei: Impacts of external photon fields and the blazar sequence*, *Physical Review D* **90** (2014) .

[12] B. Zhang, B. Zhang, H. Sun, W. Lei, H. gao, Y. Li et al., *A peculiar low-luminosity short gamma-ray burst from a double neutron star merger progenitor*, *Nature Communications* **9** (2018) .

[13] K. Murase, *High energy neutrino early afterglows from gamma-ray bursts revisited*, *Physical Review D* **76** (2007) .

[14] L. Pyras and I. Plaisier for RNO-G, *The Radio Neutrino Observatory Greenland: Status Update and Prospect for Air Showers*, *PoS ECRS2022* **in preparation** .

[15] J. van Santen, B. Clark, R. Halliday, S. Hallmann and A. Nelles, *toise: a framework to describe the performance of high-energy neutrino detectors*, *Journal of Instrumentation* **17** (2022) T08009.

Full Author List: RNO-G Collaboration

J. A. Aguilar[1], P. Allison[2], D. Besson[3], A. Bishop[4], O. Botner[5], S. Bouma[6], S. Buitink[7], M. Cataldo[6], B. A. Clark[8], K. Couberly[3], Z. Curtis-Ginsberg[9], P. Dasgupta[1], S. de Kockere[10], K. D. de Vries[10], C. Deaconu[9], M. A. DuVernois[4], A. Eimer[6], C. Glaser[5], A. Hallgren[5], S. Hallmann[11], J. C. Hanson[12], B. Hendricks[13], J. Henrichs[11,6], N. Heyer[5], C. Hornhuber[3], K. Hughes[9], T. Karg[11], A. Karle[4], J. L. Kelley[4], M. Korntheuer[1], M. Kowalski[11,14], I. Kravchenko[15], R. Krebs[13], R. Lahmann[6], U. Latif[10], J. Mammo[15], M. J. Marsee[16], Z. S. Meyers[11,6], K. Michaels[9], K. Mulrey[17], M. Muzio[13], A. Nelles[11,6], A. Novikov[18], A. Nozdrina[3], E. Oberla[9], B. Oeyen[19], I. Plaisier[6,11], N. Punsuebsay[18], L. Pyras[11,6], D. Ryckbosch[19], O. Scholten[10,20], D. Seckel[18], M. F. H. Seikh[3], D. Smith[9], J. Stoffels[10], D. Southall[9], K. Terveer[6], S. Toscano[1], D. Tosi[4], D. J. Van Den Broeck[10,7], N. van Eijndhoven[10], A. G. Vieregg[9], J. Z. Vischer[6], C. Welling[9], D. R. Williams[16], S. Wissel[13], R. Young[3], A. Zink[6]

[1]ULB Brussels, Université Libre de Bruxelles, Science Faculty CP230, B-1050 Brussels, Belgium
[2]Ohio State University, Dept. of Physics, Center for Cosmology and AstroParticle Physics, Ohio State University, Columbus, OH 43210, USA
[3]University of Kansas, University of Kansas, Dept. of Physics and Astronomy, Lawrence, KS 66045, USA
[4]University of Wisconsin-Madison, Wisconsin IceCube Particle Astrophysics Center (WIPAC) and Dept. of Physics, University of Wisconsin-Madison, Madison, WI 53703, USA
[5]Uppsala University, Uppsala University, Dept. of Physics and Astronomy, Uppsala, SE-752 37, Sweden
[6]Friedrich-Alexander-University Erlangen-Nürnberg, Erlangen Center for Astroparticle Physics (ECAP), Friedrich-Alexander-University Erlangen-Nürnberg, 91058 Erlangen, Germany
[7]VUB Brussels, Vrije Universiteit Brussel, Astrophysical Institute, Pleinlaan 2, 1050 Brussels, Belgium
[8]Michigan State University, Dept. of Physics and Astronomy, Michigan State University, East Lansing MI 48824, USA
[9]University of Chicago, Dept. of Physics, Enrico Fermi Inst., Kavli Inst. for Cosmological Physics, University of Chicago, Chicago, IL 60637, USA
[10]Vrije Universiteit Brussel, Vrije Universiteit Brussel, Dienst ELEM, B-1050 Brussels, Belgium
[11]DESY, Deutsches Elektronen-Synchrotron DESY, Platanenallee 6, 15738 Zeuthen, Germany
[12]Whittier College, Whittier College, Whittier, CA 90602, USA
[13]Penn State University, Dept. of Physics, Dept. of Astronomy & Astrophysics, Penn State University, University Park, PA 16801, USA
[14]HU Berlin, Institut für Physik, Humboldt-Universität zu Berlin, 12489 Berlin, Germany
[15]University of Nebraska-Lincoln, Dept. of Physics and Astronomy, Univ. of Nebraska-Lincoln, NE, 68588, USA
[16]University of Alabama, Dept. of Physics and Astronomy, University of Alabama, Tuscaloosa, AL 35487, USA
[17]Radboud University, Dept. of Astrophysics/IMAPP, Radboud University, PO Box 9010, 6500 GL, The Netherlands
[18]University of Delaware, Dept. of Physics and Astronomy, University of Delaware, Newark, DE 19716, USA
[19]Ghent University, Ghent University, Dept. of Physics and Astronomy, B-9000 Gent, Belgium
[20]University of Groningen, Kapteyn Institute, University of Groningen, Groningen, The Netherlands

PoS(ARENA2022)008